Ex vivo and in vivo CRISPR/Cas9 screenings identify the roles of protein N-glycosylation in regulating T-cell activation and functions

Yu Hong[1, 2, 5], Xiaofang Si[1, 2, 3, 5], Wenjing Liu[1, 2, 3, 5], Xueying Mai[1, 2, 4, 5], Yu Zhang[1, 2, 3, 4 *]

[1]Institute for Cancer Research, Chinese Institutes for Medical Research, Beijing 100069，China

[2]National Institute of Biological Sciences, Beijing 102206, China;

[3]Chinese Academy of Medical Sciences & Peking Union Medical College, Beijing 100730, China;

[4]Capital Medical University, Beijing 100069, China.

[5]These authors contributed equally to this work.

*Correspondence should be addressed to Y. Z. (zhangyu@cimrbj.ac.cn ; zhangyu@nibs.ac.cn).

Abstract

Cytotoxic $CD8^+$ T-cells play central roles in tumor immunotherapy. Understanding mechanisms that regulate development, differentiation, and functions of cytotoxic $CD8^+$ T-cells leads to development of better immunotherapies. By combining primary T-cell culture and a syngeneic mouse tumor model with both genome-wide and custom CRISPR/Cas9 screenings, we systematically identified genes and pathways that regulate PD-1 expression and functions of $CD8^+$ T-cells. Among them, inactivation of a key enzyme in glycoconjugate biosynthesis, beta 1, 4-galatosyltransferase 1 (B4GALT1), leads to significantly enhanced T-cell receptor (TCR) activation and functions of $CD8^+$ T-cell. Interestingly, suppression of B4GALT1 enhances functions of TCR-T-cells, but has no effect on chimeric antigen receptor T (CAR-T) cells. We systematically identified the substrates of B4GALT1 on $CD8^+$ T-cell surface by affinity purification and mass spectrometry analysis, which include protein components in both TCR and its co-receptor complexes. The galactosylation of TCR and CD8 leads to reduced interaction between TCR and CD8 that is essential for TCR activation. Artificially tethering TCR and CD8 by a TCR-CD8 fusion protein could bypass the regulation of B4GALT1 in $CD8^+$ T-cells. Finally, the expression levels of B4GALT1 normalized to tumor infiltrated $CD8^+$ T-cells in tumor microenvironment are significant and negatively associated with prognosis of human patients. Our results reveal the important roles of protein N-glycosylation in regulating functions of $CD8^+$ T-cells and prove that B4GALT1 is a potential target for tumor immunotherapy.

Introduction

Cytotoxic $CD8^+$ T-cells play a central role in tumor immunotherapy. The presence and activation status of $CD8^+$ T-cells in tumors are efficient biomarkers to predict prognostic and therapeutic efficacy for patients receiving immunotherapy[1, 2]. Immune checkpoint inhibitors (e.g., anti-PD-1, anti-PD-L1, and anti-CTLA4 antibodies) targeting the reactivation of tumor-infiltrated cytotoxic $CD8^+$ T-cells have shown amazing clinical benefits in treating various human tumors[3-7]. Chimeric antigen receptor T (CAR-T) and T-cell receptor-engineered T (TCR-T) cells, which are exogenous cytotoxic $CD8^+$ T-cells that are genetically engineered to directly target cancer cells, have demonstrated promising clinical efficacy against some human tumors[8, 9]. Fully elucidating the mechanisms regulating development, differentiation, and functions of cytotoxic $CD8^+$ T-cells paves ways for development of better tumor immunotherapies.

Expression of programmed cell death protein 1 (PD-1) can be induced in a wide variety of immune cell types[10-12]. For example, TCR activation induces the expression of PD-1 on T-cell surface. The interaction between PD-1 receptor and its ligand, PD-L1, reduces TCR signals to suppress immune system. When tumors evade attacks from the immune system, cancer cells upregulate their surface PD-L1 expression to prevent attack by endogenous cytotoxic $CD8^+$ T-cells. Antibodies blocking the interaction between PD-1 and PD-L1 have been proven to be effective in human tumor immunotherapy and show high efficacy in many tumor types[4, 5]. Understanding how immune cells regulate their PD-1 expression is one of the most important aspects of tumor immunology research. Although a few regulators of PD-1 expression in cytotoxic $CD8^+$ T-cells have been identified recently[13-17], an unbiased systematic screening is still missing.

Here, by combining ex vivo primary memory $CD8^+$ T-cell culture and an in vivo syngeneic mouse tumor model with genome-wide and custom CRISPR/Cas9

screenings, we systematically identified genes and pathways that regulate PD-1 expression and functions of $CD8^+$ T-cells. Among them, inactivation of a key enzyme in glycoconjugate biosynthesis, i.e., B4GALT1, enhances PD-1 expression, TCR activation, and functions of mouse $CD8^+$ T-cells both in vitro and in vivo. Similar roles of B4GALT1 were also observed in human $CD8^+$ T-cells. Mechanistic studies indicate that B4GALT1 regulates $CD8^+$ T-cell function via a TCR-dependent pathway through cell surface protein glycosylation. Systematic LC-MS analysis further identified that proteins in TCR-complex and its co-receptors are direct substrates of B4GALT1. Mechanistic studies indicate that B4GALT1 deficient T-cells showed stronger TCR-CD8 interaction and enhanced TCR activation than wild-type control, which can be bypassed by artificially tethering of TCR with CD8 when a CD8β-CD3ε fusion protein was overexpressed. These results support a model that B4GALT1 modulates T-cell functions by direct galactosylation of TCR and CD8 which prevents the interaction between them. Finally, the expression of B4GALT1 showed a significant negative correlation with prognosis of human cancer patients when normalized to tumor infiltrated $CD8^+$ T-cells. Taken all together, the results reveal the important roles of protein N-glycosylation in regulating functions of $CD8^+$ T-cells and prove that B4GALT1 is a potential target for tumor immunotherapy.

Results

Ex vivo and in vivo CRISPR/Cas9 screenings identify genes and pathways that regulate PD-1 expression and functions of $CD8^+$ T-cells

We set up an ex vivo genome-wide CRISPR/Cas9 screening system to identify genes and pathways that regulate PD-1 expression in mouse primary $CD8^+$ T-cells (Fig. 1a). In brief, splenic $CD8^+$ T-cells from Cas9-EGFP/OT-I mice were infected with a retroviral whole-genome guide RNA (gRNA) library following ovalbumin (Ova) peptide stimulation. After puromycin selection, the memory $CD8^+$ T-cells were re-stimulated by co-culturing with B16F10-OVA cells. The highest and lowest 5% PD-1^+ cells were isolated by fluorescence-activated cell sorting (FACS) and defined as PD-1^{high} and PD-1^{low} populations, respectively (Fig. S1a). The distributions of individual gRNAs in the whole-genome library in those subpopulations, as well as in input cells, were revealed by next-generation sequencing. As shown in Fig. 1b, *Pdcd1* and previously identified PD-1 regulators, such as *Satb1*[14] and *Fut8*[15], were successfully identified as positive controls. The top candidates were verified by single sgRNA knockout (Fig. S2), and most of them showed matched results as in screenings both at RNA and cell surface protein expression levels (Fig. 1c). Gene set enrichment analysis (GSEA) identified several KEGG (Kyoto Encyclopedia of Genes and Genomes) pathways significantly involved in regulation of PD-1 expression in $CD8^+$ T-cells (Fig. 1d). As expected, genes that are known to be involved in the T-cell receptor (TCR) activation pathway such as *Cd3d*, *Zap70*, and *Lat* were among the top ones identified. Interestingly, genes involved in protein export pathway (such as *Srp14*, *Srp68*, *Sec16A*) and in aminoacyl tRNA biosynthesis (such as *Mars*, *Hars2*, *Eprs*) were significantly increased in PD-1^{low} populations. In addition, we also identified and verified genes required for N-glycan biosynthesis, including *B4galt1*, *Mgat2*, and *Dpm3*, which could negatively regulate the expression of PD-1 (Fig. S1b-d).

To verify these candidate genes in a high-throughput manner, we synthesized a

custom gRNA library containing 4,617 gRNAs targeting the top candidate genes obtained from whole-genome screenings and 105 intergenic control gRNAs. The gRNA library-infected Cas9-EGFP/OT-I memory $CD8^+$ T-cells were restimulated by co-culture and PD-1 regulators were enriched using the same strategy as whole-genome screening (Fig. 1a). As shown in Fig. 2b, most of the significant PD-1 regulators in the top list of genome-wide screening could also be enriched in the custom small library screening, which indicates the reliability of our ex vivo screenings. To test potential functions of these candidate genes in the context of tumor microenvironment, custom gRNA-library-infected Cas9-EGFP/OT-I memory $CD8^+$ T-cells were transplanted into wild-type (WT) C57BL/6J mice inoculated subcutaneously (s.c.) with B16F10-OVA tumors to screen for genes regulating $CD8^+$ T-cell functions in vivo. After 7 days, tumor-infiltrated $CD8^+$ T-cells were collected for gRNA sequencing (Fig. 2a). We successfully identified several positive control genes[18-21] such as *Socs1*, *Regnase-1 (Zc3h12a)*, *Rc3h1*, and *Cd36*, indicating our in-vivo screening system worked robustly (Fig. 2c). Interestingly, inactivating *B4galt1*, which encodes beta-1,4-galactosyltransferase 1, showed significant phenotypes in both ex vivo and in vivo screenings.

<u>B4GALT1 suppression in $CD8^+$ T-cells activates TCR signaling and enhances T-cell functions both in vitro and in vivo</u>

B4GALT1 is one of the seven beta-1,4-galactosyltransferases that transfer galactose in a beta 1-4 linkage to similar acceptor sugars, including N-acetylglucosamine (GlcNAc), glucose (Glc), and xylose (Xyl). More specifically, B4GALT1 uses UDP-galactose and N-acetylglucosamine for the production of galactose beta-1,4-N-acetylglucosamine[22]. In addition to glycoconjugate biosynthesis, B4GALT1 can also form a heterodimer with a-lactalbumin (LALBA) as lactose

synthetase in lactating tissues. Although B4GALT1 is expressed ubiquitously, its roles in regulating interaction and adhesion of immune cells have been suggested[23-28].

Infection of Cas9-EGFP/OT-I $CD8^+$ T-cells with different single gRNAs targeting B4galt1 resulted in significantly increased surface PD-1 expression and PD-1 mRNA levels both before and after co-culture with B16F10-OVA cells (Fig. 3a and Fig. S1d). Such phenotypes could be rescued by overexpression of either a short or long isoform of mouse *B4galt1* cDNA (Fig. 3b), suggesting that biosynthetic function, but not ligand-induced signal transduction, of B4GALT1[22] is responsible for suppression of PD-1 expression. In addition, *B4galt1* deficient OT-I T-cells showed enhanced expression of T-cell activation and cytotoxic markers such as IFNγ and TNFα (Fig. 3c), as well as in vitro targeted cell killing activity when co-cultured with target cells, B16F10-OVA (Fig. 3d). To verify whether B4GALT1 has similar functions in human T-cells, we infected primary human $CD8^+$ T-cells with NY-ESO-1 TCR constructs containing shRNA expression cassettes targeting human B4GALT1[29] (Fig. 3e). As shown in Fig 3f, comparing with control, knockdown of human B4GALT1 enhanced targeted killing of human A375 cells in vitro. Increased secretion levels of IFNγ and TNFα have been observed after knockdown of B4GALT1 (Fig. 3g). Surprisingly, knockout of B4GATL1 could not affect hCD19-CAR mediated in vitro killing of Nalm6 cells (Fig. S3). When stimulate with only anti-CD3/28 antibodies in the absence of target cells, B4GALT1 knockout OT-I cells also did not show significantly enhanced expression of IFNγ and TNFα, comparing with controls (Fig. S4). These results indicate that B4GALT1 may enhance T-cell functions via a TCR- and target-cell dependent pathway.

To dissect mechanisms by which B4GALT1 regulates T-cell functions, we sorted OT-I T-cells after co-culture with target cells for genome-wide transcriptional analysis. Whole-genome RNA sequencing analysis confirmed the enhanced TCR activation in *B4galt1* knockout $CD8^+$ T-cells (Fig. 3h-j). GSEA of DEGs (differentially expressed

genes) between control and *B4galt1* gRNA-infected $CD8^+$ T-cells revealed that TCR signaling pathway was at the top of significantly altered pathways (Fig. 3j).

When transplanted into wild-type mice with B16F10-OVA cells inoculated subcutaneously, *B4galt1* gRNA-infected OT-I T-cells showed significantly higher tumor killing activity than control gRNA-infected cells (Fig. 4a-c). Analysis of tumor-infiltrated lymphocytes (TILs) demonstrated more infiltrated OT-I T-cells in tumors when *B4galt1* gRNA was infected (Fig. 4d, Fig. S5). Mechanistically, B16F10-OVA tumors had similar numbers of infiltrated *B4galt1* gRNA-infected OT-I T-cells as control gRNA-infected cells 24 hours after intravenous injection (Fig. S6a), suggesting that B4GALT1 has no significant effect on initial tumor infiltration of OT-I T-cells. On the other hand, CFSE (carboxyfluorescein succinimidyl ester) analysis at a later time point (6 days after infusion) showed increased OT-I T-cell proliferation within tumors when B4GALT1 was inactivated (Fig. S6b). Altogether, these results suggest that inhibition of N-galactosylation could enhance functions of $CD8^+$ T-cells both in vitro and in vivo, and that B4GALT1 could be a potential target to modulate activity of T-cells.

<u>Systematically identification of direct substrates of B4GALT1 on T-cell surface</u>

To dissect the molecular mechanism by which B4GALT1 regulates T-cell activation, we analyzed N-glycome on OT-I T-cell surface by FACS staining (Fig. S7a). Biotin-labeled *Erythrina cristagalli* lectin (ECL) and succinyl-wheat germ agglutinin (sWGA) were used to profile surface expression of terminal βGal and βGlcNAc, respectively. *B4galt1* knockout OT-I T-cells showed slightly but significantly decreased ECL staining and significantly increased sWGA staining, comparing with control T-cells (Fig. S7b-c). FACS staining with biotin-labeled recombinant Galectin-1 (Gal-1) showed a more dramatic difference between control and *B4galt1* knockout OT-I T-cells (Fig. S7d).

To identify potential substrates of B4GALT1 on $CD8^+$ T-cell surface, we used a recombinant Gal-1 affinity column and lactose elution to purify N-glycosylated proteins from whole membrane-protein extracts of OT-I $CD8^+$ T-cells (Fig. 5a). LC-MS analysis of proteins that were significantly different between control and *B4galt1* knockout OT-I T-cells revealed that both TCRα/β (OT-I) and CD8α/β were among the top list (Fig. 5b). KEGG analysis also showed a significant enrichment of TCR signaling pathway (Fig. 5c). We could verify reduced Gal-1 pull-down for CD8β and most of other hits in *B4galt1* knockout T-cells by western blotting with commercially available antibodies (Fig. 5d). Interestingly, migration of CD8β in SDS-PAGE was significantly different between control and *B4galt1* knockout T-cell extracts, suggesting that CD8β is a direct substrate of B4GALT1 (Fig. 5d). Indeed, treating whole membrane-protein extracts with PNGase F to remove all N-linked glycosylation on proteins omitted the migration difference of CD8β and most of other hits we identified (Fig. 5e). These results suggest that B4GALT1 directly regulates N-glycosylation of cell surface proteins, such as components of TCR and CD8 complexes, on $CD8^+$ T-cell.

It has been suggested that interaction between TCR and CD8 plays an important role for TCR activation[30, 31]. We hypothesized that aberrant galactosylation of TCR and CD8 might directly affect their interaction. For that, we used a FRET (Fluorescence Resonance Energy Transfer) assay to measure interaction between TCR and CD8[30, 31] (Fig. S8). As shown in Fig. 5f, FRET signals of TCR-CD8 increased significantly in B4GALT1 deficient T-cells, comparing with control T-cells. To confirm that reduced TCR-CD8 interaction is the major cause of TCR activation phenotypes in B4GALT1 knockout $CD8^+$ T-cells, we generated a construct which fused the CD8β ectodomain (ECD) with CD3ε (Fig.5g). We expected that such fusion could artificially tether TCR with CD8, and bypass the regulation by B4GALT1. Indeed, overexpression of the CD8β-CD3ε fusion led to enhanced in vitro killing activities in control $CD8^+$ T-cells. On the other hand, in

B4GALT1 deficient $CD8^+$ T-cells, such enhanced T-cell killing activities by fusion construct was significantly diminished (Fig.5h). Taken together, these results support a model that B4GALT1 directly regulates galactosylation of TCR complex and co-receptors to regulate TCR-CD8 interaction, which is essential for TCR activation and functions of T-cells.

The expression levels of B4GALT1 and tumor infiltrated $CD8^+$ T-cells in tumor microenvironment are associated with prognosis of human patients

To investigate potential clinical relevance of B4GALT1 in human tumor patients, we analyzed cancer samples in The Cancer Genome Atlas (TCGA)[32]. While expression levels of B4GALT1 are not linked to an overall survival benefit using data of all TCGA collected primary cancer samples, after normalized to expression level of CD8A, Kaplan-Meier curve showed a significantly better survival duration in patients with low expression of B4GALT1 (Fig. S9a-b)[33]. In Adrenocortical carcinoma (ACC), Acute Myeloid Leukemia (LAML), Lung adenocarcinoma (LUAD), and Rectum adenocarcinoma (READ) data sets, for patients with higher expression of CD8A, low B4GALT1 expression level is significantly associated to better overall survival, comparing with patients with lower expression of CD8A (Fig. 6a and Fig. S9c). On the contrary, in patients with lower expression of B4GALT1, high CD8A expression level is significantly associated to better overall survival, comparing with patients with higher expression of B4GALT1 (Fig. 6b and Fig. S9c). Collectively, these data suggest expression of B4GALT1 in tumor microenvironment and presence of tumor infiltrated $CD8^+$ T-cells are jointly associated with prognosis of cancer patients.

Discussion

Cytotoxic CD8$^+$ T-cells, which directly kill tumor cells, are key effector cells within tumor microenvironment[34, 35]. Following TCR activation by MHC-peptide complexes, PD-1 expression in T-cells is significantly upregulated[36, 37]. Cytokines, such as IL-2, IL-7, and interferons secreted by T-cells, can also induce high PD-1 expression[38]. Beyond its role as one of the markers for TCR activation, PD1 suppresses further T-cell activation after binds to its ligand PD-L1, thereby preventing excessive immune responses[39]. Therapeutically targeting PD-1 molecules on immune cells, especially cytotoxic CD8$^+$ T-cells, is one of the most successful strategies to treat tumors[5]. Understanding the mechanisms that regulate PD-1 expression on cytotoxic CD8$^+$ T-cells presents important clues to optimize current tumor immunotherapy strategies, including CAR-T/TCR-T and immune checkpoint inhibitors, especially anti-PD-1 and anti-PD-L1 blocking antibodies.

By genome-wide CRISPR/Cas9 screenings, we systematically identified genes and pathways regulating PD-1 expression in primary CD8$^+$ T-cells. In such ex vivo T-cell activation system, PD-1 serves mainly as an early activation marker for TCR. It will be interesting to adapt T-cell exhaustion culture with current screenings, where PD-1 is induced as an exhaustion marker[40-42]. The results that *Pdcd1* gene and some previously reported regulators of PD-1, such as *Satb1* and *Fut8*, were successfully identified, demonstrate the effectiveness of this screening system. Interestingly, genes in N-glycan biosynthesis are significantly enriched to negatively regulate PD-1 expression in CD8$^+$ T-cells. Inhibition of B4GALT1 could activate expression of PD-1 and functions of CD8$^+$ T-cells both in vitro and in vivo. Mechanistically, B4GALT1 modulates galactosylation of proteins on CD8$^+$ T-cell surface, including proteins in TCR complex and its co-receptors. The decreased galactosylation of TCR complex and CD8 enhances TCR-CD8 interaction, which is the major downstream mechanism that B4GALT1 regulates TCR activation. Our results not only demonstrate the

important roles of protein N-glycosylation in regulating functions of $CD8^+$ T-cells but also prove that B4GALT1 is an effective target for tumor immunotherapy. In particular, previous studies have demonstrated the roles of B4GALT1 in cancer cells such as in LUAD and CRC[26-28]. Our study suggests that inhibition of B4GALT1 in both cancer cells and $CD8^+$ T-cells may synergistically suppress tumor growth.

Based on results from individual studies of specific glycosidases and glycosyltransferases, N-linked glycosylation of T-cell surface proteins have been proposed to regulate T-cell development, activation, and functions[43]. Here, we identified roles of N-glycome synthesis in regulating PD1 expression of $CD8^+$ T-cells by unbiased genome-wide screenings. To further investigate mechanisms, we systematically characterized substrates of B4GALT1 on $CD8^+$ T-cell surface, suggesting the model that B4GALT1 regulates TCR activation by directly modulate N-glycosylation of components of TCR and its co-receptor complexes. In addition, several interesting observations also provides mechanistic insights supporting our hypothesis. Knockout of B4GALT1 only significantly affect activation of exogenous and exogenous TCR (OT-I and NY-ESO-1, respectively) but not CAR (hCD19-CAR) in $CD8^+$ T-cells. Similarly, knockout of CD8a shows different effect on TCR and CAR activation (data not shown). Moreover, different from results obtained after co-culture with target cells, when B4GALT1 knockout $CD8^+$ T-cells were stimulated by anti-CD3/28 only, they did not show significantly enhanced activation. Further studies are necessary to clarify whether B4GALT1 mediated N-galactosylation modifications directly or indirectly affect functions of its other substrates and how cancer cells contribute to activation of $CD8^+$ T-cells in a B4GALT1-dependent manor.

Adoptive T-cell therapy has been actively implicated for treatment of cancer and chronic infections[44, 45]. While CAR-T and TCR-T therapies demonstrated promising effect in controlling hematological malignancies, their applications in solid tumors remains challenging[46, 47]. How to enhance activities of in vitro expanded T-cells is

also a major barrier for tumor-infiltrating lymphocyte (TIL) therapy[48]. Our in vitro and in vivo results strongly support that B4GALT1 is a potential target to enhance the efficacy of adoptive T-cell therapy.

In summary, our study utilized unbiased genome-wide and custom small library screenings to identify PD-1 regulators in $CD8^+$ T-cells, and discovered a fundamental role for a gene involved in N-glycan biosynthesis---B4GALT1, which can enhance T-cell activation and functions both in vitro and in vivo. Our findings highlight the power of protein N-glycosylation in regulating functions of $CD8^+$ T-cells and suggest that B4GALT1 is a potential target for tumor immunotherapy. It will provide a new perspective and direction for the research of T-cell regulators to enhance the efficacy of tumor immunotherapy.

Declarations

Ethics approval and consent to participate

All animal experiments were conducted following the Ministry of Health national guidelines for housing and care of laboratory animals and performed in accordance with institutional regulations after review and approval by the Institutional Animal Care and Use Committee at the National Institute of Biological Sciences and Chinese Institutes for Medical Research. The assigned approval/accreditation number: AEEI-2023-223.

This manuscript does not report on or involve the use of any human data or tissue.

Consent for publication

This manuscript does not contain data from any individual person.

Availability of data and materials

The raw sequence data reported in current study have been deposited in the Genome Sequence Archive in BIG Data Center, Beijing Institute of Genomics (BIG), Chinese Academy of Sciences, under accession numbers PRJCA010494 that can be accessed at https://ngdc.cncb.ac.cn/search/?dbId=&q=PRJCA010494.

Other materials used during the current study are available from the corresponding author on reasonable request.

Competing interests

Part of this research has been submitted for a patent.

Funding

The research in Y.Z. lab is supported by grants from National Key R&D Program of China (2021YFA1101002), National Natural Science Foundation of China (81773304,

81572795), the “Hundred, Thousand and Ten Thousand Talent Project” by Beijing municipal government (2019A39).

Authors' contributions

Y.H. and Y.Z. conceived the study. Y.H., X.S., W.L., X.M. performed experiments and analyzed data. Y.Z. analyzed data and wrote the manuscript with support from all authors.

Acknowledgments

We thank members of Y.Z. lab for helpful discussion and support. We thank the core facility center at Capital Medical University (CMU) for helpful assistance and service. We thank the municipal government of Beijing and the Ministry of Science and Technology (MOST) of China for funds allocated to NIBS, and the municipal government of Beijing for funds allocated to CIMR.

Figure legends:

Figure 1. Ex vivo CRISPR/Cas9 screenings identify genes and pathways that regulate PD-1 expression of CD8$^+$ T-cells.

a. Schematic view of ex vivo CRISPR/Cas9 screening in mouse primary CD8$^+$ T-cells.
b. Volcano plot showing results of ex vivo CRISPR/Cas9 genome-wide screenings. The p-values were calculated using the α-robust rank aggregation (α-RRA) algorithm in MAGeCK.
c. Verification of candidate genes by individual single gRNAs. The relative expression levels of surface PD-1 protein and PD-1 mRNA were measured by FACS as mean fluorescent intensity (MFI) and RT-qPCR, respectively.
d. GSEA of significantly enriched KEGG pathways in genome-wide screening. The enrichment score (ES) and statistical significance were calculated using the clusterProfiler (version 3.12.0) R package.

Figure 2. In vivo CRISPR/Cas9 screenings with a custom gRNA library identify genes that regulate functions of CD8$^+$ T-cells in tumor microenvironment.

a. Schematic view of in vivo CRISPR/Cas9 screening in mouse primary CD8$^+$ T-cells.
b. Volcano plot showing results of ex vivo CRISPR/Cas9 screening. The p-values were calculated using the α-RRA algorithm in MAGeCK.
c. Volcano plot showing results of in vivo CRISPR/Cas9 screenings. The p-values were calculated using the α-RRA algorithm in MAGeCK.

Figure 3. B4GALT1 suppression in CD8$^+$ T-cells activates TCR signaling and enhances T-cell functions.

a. CRISPR/Cas9 knockout of *B4galt1* (sgB4galt1) (sg2) in CD8$^+$ T-cells increases expression of PD-1 before and after co-culture with B16F10-OVA cells. The MFIs

of PD-1 were measured by FACS. The relative mRNA levels of PD-1 were measured by quantitative RT-qPCR. The p-values were calculated using a two-tailed Student's t-test.

b. The effect of *B4galt1* knockout on PD-1 surface expression could be rescued by overexpression of either long- or short-isoform B4galt1. The p-values were calculated using a two-tailed Student's t-test.

c. CRISPR/Cas9 knockout of *B4galt1* in $CD8^+$ T-cells increases expression of TNFα and IFNγ after co-culture with B16F10-OVA cells. The relative mRNA levels were measured by quantitative RT-qPCR. The secreted TNFα and IFNγ in medium were measured by ELISA. The p-values were calculated using a two-tailed Student's t-test.

d. CRISPR/Cas9 knockout of *B4galt1* in OT-I $CD8^+$ T-cells increases in vitro specific killing activities on B16F10-OVA cells. The p-values were calculated using a two-tailed Student's t-test.

e. Schematic view of B4GALT1 knockdown in human NY-ESO-1 TCR-T-cells.

f. Knockdown of B4GALT1 in human NY-ESO-1 TCR-T-cells by shRNA increases in vitro killing activities on A375 cells. The p-values were calculated using a two-tailed Student's t-test.

g. Knockdown of B4GALT1 in human NY-ESO-1 TCR-T-cells increases expression of TNFα and IFNγ after co-culture with A375 cells. The secreted TNFα and IFNγ in medium were measured by ELISA. The p-values were calculated using a two-tailed Student's t-test.

h. Heatmap demonstrating differentially expressed genes (DEGs) between B4galt1 knockout and control mouse OT-I $CD8^+$ T-cells after co-culture. The genes in TCR signaling pathway are labeled on the left side.

i. Volcano plot showing upregulated and downregulated genes (p-value<0.01) in B4galt1 knockout mouse OT-I $CD8^+$ T-cells after co-culture. The genes in TCR signaling pathway are labeled with dark blue and dark red. Top genes and some

genes in TCR signaling pathway are annotated. The p-value was calculated using the Wald test, and p.adjust was calculated using Benjamini-Hochberg with the R package DESeq2 (version 1.22.2).

j. Bar graph showing KEGG pathways significantly changed in *B4galt1* knockout mouse OT-I $CD8^+$ T-cells after co-culture. The p-value was calculated using the clusterProfiler (version 3.12.0) R package.

Data are shown as the mean ± SEM. *P < 0.05; **P < 0.01; ***P < 0.001.

Figure 4. Knockout of *B4galt1* in $CD8^+$ T-cells enhances T-cell-mediated tumor immunotherapy.

a. Schematic view of *B4galt1* functional test in tumor microenvironment.
b. CRISPR/Cas9 knockout of B4galt1 in OT-I T-cells enhances growth control of B16F10-OVA tumors in vivo. The p-value was calculated using two-way ANOVA.
c. Compared with control OT-I T-cells, the tumors were significantly smaller when B4galt1 knockout OT-I T-cells were transplanted. The p-value was calculated using a two-tailed Student's t-test.
d. CRISPR/Cas9 knockout of B4galt1 increases numbers of OT-I T-cells in B16F10-OVA tumors. The p-value was calculated using a two-tailed Student's t-test.

Data are shown as the mean ± SEM. *P < 0.05; **P < 0.01.

Figure 5. Systematic identification of direct substrates of B4GALT1 on T-cell surface.

a. Schematic view of recombinant Gal-1 pulldown and LC-MS experiments.
b. Volcano plot showing identified Gal-1 binding proteins in control and B4galt1 knockout OT-I cells. Proteins among the top list were annotated and labeled with red (decreased in *B4galt1* knockout) and green (increased in *B4galt1* knockout). Proteins in TCR signaling pathway are underlined. The p-values were calculated

using Limma in DEqMS (V1.8.0).

c. Bar graph showing KEGG pathways significantly changed in *B4galt1* knockout OT-I T-cells. The p-value was calculated using the clusterProfiler (version 3.12.0) R package.

d. Western blot verification of pulldown hits in top list.

e. N-glycome analysis with PNGase F suggests that CD8β is a direct substrate of B4GALT1.

f. Compared with wild-type control, B4GALT1 knockout OT-1 T-cells showed significantly stronger TCR-CD8 FRET signals.

g. Schematic view of the CD8β-CD3ε fusion construct.

h. Overexpression of a CD8β-CD3ε fusion protein bypassed the effect of B4GALT1 on T-cell in vitro killing activities.

All of the p-values were calculated by a two-tailed Student's t test. Data are shown as the mean ± SEM. *P < 0.05; **P < 0.01; ***P < 0.001; NS, not significant.

Figure 6. The expression levels of B4GALT1 and tumor infiltrated CD8$^+$ T-cells in tumor microenvironment are associated with prognosis of human patients.

a. The association between B4GALT1 expression levels and overall survival for patients with different CD8A levels in TCGA-ACC, -LAML, -LUAD, and -READ cohorts.

b. The association between CD8A expression levels and overall survival for patients with different B4GALT1 levels in TCGA-ACC, -LAML, -LUAD, and -READ cohorts.

The p-values for all survival curves were calculated using two-sided Log-rank test.

Methods

Cell lines

HEK293T cell line was purchased from ATCC. B16F10 cell line was provided by laboratory of Dr. Ting Chen (National Institute of Biological Sciences, Beijing). Nalm6 cell line was provided by laboratory of Dr. Zhaoqing Ba (National Institute of Biological Sciences, Beijing). A375 cell line was provided by laboratory of Dr. Feng Shao (National Institute of Biological Sciences, Beijing). B16F10-OVA cell line was constructed by infecting B16F10 cells with lentivirus encoding chicken ovalbumin.

B4galt1 rescue vectors were constructed based on pMSCV-U6 sgB4galt1-PGK-puro-2A-BFP vector. Long isoform (UniProt, P15535-1) and short isoform (UniProt, P15535-2) were amplified from cDNA of mouse T-cells, and used to replace the BFP fragment by seamless cloning kit (Biomed, CL116).

The CD8β-CD3ε fusion vector was constructed by fusing CD8β ectodomain (ECD) and its signal peptide with, a linker region, and the full-length of CD3ε, based on pMSCV-U6 sgB4galt1/empty-PGK-puro-2A-BFP vector mentioned above.

HEK293T, B16F10 and A375 cells were cultured in DMEM (Gibco C11965500BT) supplemented with 10% fetal bovine serum (FBS), 2 mmol L-glutamine, 100 μg/ml penicillin, and 100 U/ml streptomycin (all purchased from Gibco). Nalm6 cells were maintained in RPMI-1640 (HyClone) medium supplemented with 15% FBS, 100 μg/ml penicillin, 100 U/ml streptomycin, 10 mM HEPES, 0.1 mM 2-mercaptoethanol, 2 mM L-glutamine and 1xMEM nonessential amino acids.

Retrovirus and lentivirus preparation

Retrovirus was packaged by co-transfecting HEK293T cells with MSCV vector and pCL-Eco. 48 hours post-transfection, supernatant was collected and filtered through a 0.45 μm filter to remove cell debris. Virus was then concentrated by centrifugation in Beckman Optima L-100XP (SW32Ti) at 25,000 rpm (107,000 g) for 2.5 hours at 4 °C

and resuspended in RPMI-1640 basic medium.

Lentivirus was packaged by co-transfecting HEK293T cells with lentiviral vector, psPAX2, and pMD2.G. 48 hours post-transfection, supernatant was collected and filtered through a 0.45 μm filter to remove cell debris. Virus was used for infection directly or concentrated by centrifugation at 25,000 rpm (107,000 g) for 2.5 hours at 4 °C and resuspended in PBS.

To produce lentivirus for human $CD8^+$ T-cell infection, HEK293T cells were seeded in Opti-MEM I Reduced Serum Medium (Gibco, 31985-070) supplemented with 5% FBS, 1 mM sodium pyruvate (Gibco, 11360-070), and 1xMEM nonessential amino acids (Gibco, 11140-050) the day before transfection. 6 hours post-transfection, the transfection medium was replaced with fresh medium supplemented with 1x ViralBoost (Alstem Bio, VB100). Lentivirus was collected and filtered through a 0.45 μm filter 24 hours and 48 hours after transfection separately, followed by addition of Lenti-X-Concentrator (Takara, 631232). Lentivirus was concentrated following manufacturer's instructions and resuspended in X-VIVO 15 medium (Lonza, 04-418Q) in 1% of the original volume.

Animals

Female C57BL/6J mice were purchased from Beijing Vital River Laboratory Animal Technology Co., Ltd. OT-I mice were provided by laboratory of Dr. Hai Qi (Tsinghua University). Cas9-EGFP/OT-I mice were generated by breeding OT-I and Cas9-EGFP knock-in mice [49] at animal facility of the National Institute of Biological Sciences, Beijing. Six- to eight-week-old mice were used at the start of experiments. Animals were housed under specific pathogen-free conditions in individually ventilated cages in a controlled 12-h day-night cycle with standard food and water provided ad libitum. All animal experiments were conducted following the Ministry of Health national guidelines for housing and care of laboratory animals and performed in accordance with institutional regulations after review and approval by the Institutional Animal Care

and Use Committee at the National Institute of Biological Sciences.

Retroviral whole-genome CRISPR/Cas9 gRNA library construction

A whole-genome CRISPR knockout gRNA library (1000000096) was purchased from Addgene. The gRNA regions were PCR amplified with primer pair F:5'-GGCTTTATATATCTTGTGGAAAGGACGAAACACCG-3' and R:5'-CTAGCCTTATTTTAACTTGCTATTTCTAGCTCTAAAAC-3', and then transferred into MSCV-gRNA-PGK-PURO-2A-BFP vector by Gibson reaction. For knockout of individual genes, a single gRNA was cloned into the same vector by Gibson reaction.

Retroviral small custom gRNA library construction

A total of 1,398 genes were selected according to whole-genome knockout screening results. On average, three gRNAs were selected from the initial library for each gene according to gRNA performance (Supplementary Table 3). A total of 105 intergenic control gRNAs were also added. Oligonucleotides containing the guide sequence were synthesized (Custom Array), PCR-amplified, and cloned into MSCV-gRNA-PGK-PURO-2A-BFP vector via Gibson reaction.

Ex vivo T memory cell culture, infection, and adoptive transfer

On Day 0, splenocytes were prepared from 6- to 8-week-old Cas9-EGFP/OT-I female mice and cultured with IL2 (10 ng/ml) and SIINFEKL peptide (10 ng/ml) in complete RPMI media (RPMI 1640, 10% FBS, 20 mM HEPES, 1 mM sodium pyruvate, 0.05 mM 2-mercaptoethanol, 2 mM L-glutamine, 100 U/ml streptomycin, and 100 μg/ml penicillin) at a density of $1X10^6$ cells/ml for 24 hours. On day 1, activated Cas9-EGFP/OT-I T-cells were enriched by Percoll isolation as previously described[50] and spin-infected (2,000 g, 30 °C, 1 hour, with minimum acceleration and no brake) with retrovirus supplemented with polybrene (8 μg/ml) in 24-well-plate. After spin-infection, the plate was placed into a CO_2 incubator at 37 °C for 5 hours and

cultured with IL2 (2 ng/ml), IL7 (2.5 ng/ml), and IL15 (10 ng/ml) in complete RPMI media at a density of $3x10^5$ cells/ml. Two days after infection (Day 3), cells were selected by 3 μg/ml puromycin in the presence of IL2/IL7/IL15 for another 4 days. On day 7, cells were used for co-culture experiments or adoptive transfer.

Human T-cell isolation, culture and transduction

Human peripheral blood mononuclear cells (PBMC) were acquired from healthy donors. $CD8^+$ T-cells were isolated using EasySep negative selection kit (STEMCELL, Cat#17953), and stimulated with anti-CD3/CD28 Dynabeads (Thermo Fisher Scientific, Cat#40203D). T-cells were cultured in X-VIVO medium with 10% FBS, 2 mmol L-glutamine, 100 μg/ml penicillin, 100 U/ml streptomycin, and human IL2 (500 IU/ml). 48 hours after activation, T-cells were transduced in a lentivirus-coated plate, centrifuged at 1,200 g for 90 minutes at 37℃. Lentivirus transduction was repeated once 24 hours later. Positive transduced cells were sorted 3 days later. During T-cell expansion, the cells were maintained at a concentration of 3×10^5 cells/ml.

Anti-CD19-CAR and NY-ESO-1 specific TCR-T-cell generation

pMSCV-CD19 scFv (FMC63)-IRES-RFP-U6 sgRNA vector was constructed from a pMSCV-CD19 scFv-IRES-RFP vector provided by laboratory of Dr. Feng Shao (National Institute of Biological Sciences, Beijing). An U6 sgRNA cassette was assembled by seamless cloning kit (Biomed, CL116).

$CD8^+$ T-cells were purified from splenocytes of Cas9-EGFP knock-in mice by a mouse $CD8^+$ T-cell isolation kit (R&D, MAGM203). At day 0, $CD8^+$ T-cells were stimulated with anti-CD3 (1 μg/ml, Cat#14-0031-86) and anti-CD28 (0.5 μg/ml, Cat#102116) in complete RPMI 1640 medium containing 20 ng/ml IL2 for 24 hours. On day 1, activated $CD8^+$ T-cells were enriched by Percoll isolation and spin-infected (2,000 g, 30 °C, 1 hour, with no acceleration or brake) with retrovirus expressing anti-CD19-CAR and sgRNA supplemented with polybrene (8 μg/ml) in 24-well-plate. The RFP^+ cells were sorted on day 3 for further culture. $CD8^+$ T-cells were cultured

with the same condition as T memory cells. In vitro killing assay was perform on day 7 by mixing anti-CD19-CAR-T-cells with Nalm6.

NY-ESO-1 specific TCR (1G4)[29] was synthesized and cloned into a lentiviral backbone with a SFFV promoter. T2A-BFP fragment and U6 shRNA cassette were assembled by seamless cloning kit (Biomed, CL116) simultaneously.

NY-ESO-1 specific TCR-T-cells were generated following the human $CD8^+$ T-cell isolation, culture, and transduction protocols. 3 days post-transduction, BFP^+ cells were sorted for further culture. 7 days post-transduction, in vitro killing assay was performed by mixing T-cells with A375 cells.

CRISPR/Cas9 screening

For ex vivo PD-1 expression screening, at Day 6, $3x10^6$ B16F10-OVA cells were plated in 15 cm dishes in DMEM (DMEM+10% FBS+ Pen/Strep). On Day 7, puromycin-selected OT-I T-cells were resuspended in a final concentration of $6x10^5$ cells/ml with complete RPMI 1640 medium supplemented with IL2 (2 ng/ml), IL7 (2.5 ng/ml), and IL15 (10 ng/ml), and added to B16F10-OVA cells at a T-cell:B16F10-OVA cell ratio of 4:1. Cells were co-cultured overnight at 37 °C. $CD8^+$ T-cells were then collected and stained with PE anti-PD-1 in 2% FBS/PBS for 30 minutes on ice. The highest and lowest 5% $PD\text{-}1^+$ cells were sorted via BD FACSAria.

For the secondary small custom library in vivo screening, following 4-day puromycin selection, an aliquot of $2x10^6$ infected OT-I T-cells was saved as input (approximately 269X cell coverage per sgRNA). Library-infected OT-I T-cells ($2x10^6$ cells per recipient) were intravenously transferred into mice bearing Day 14 B16F10-OVA tumors. In total, 24 mice were used as recipients. At 7 days post-adoptive transfer, B16F10-OVA tumors were digested into single-cell suspensions, and tumor-infiltrated $CD8^+$ T-cells were isolated by biotin anti-mouse CD8a (Biolegend, 100704) and streptavidin beads. Meanwhile, a 1/20 volume aliquot of single-cell suspension was used for OT-I staining to estimate numbers of infiltrated OT-I T-cells in each tumor. A

total of $1x10^4$ to 1×10^5 OT-I T-cells were collected per tumor.

Sequencing library preparation

Genomic DNA was extracted by phenol/chloroform extraction. Primary PCR was performed using Titanium Taq DNA Polymerase (Clontech, 639242) to amplify the sgRNA region. A secondary PCR was performed to add adaptors and indexes to each sample. Nova-seq 150-bp paired-end sequencing (Illumina) was performed.

Analysis of screening results

Raw reads were preprocessed using sequence-grooming tools to remove adaptor sequences with Cutadapt (version 3.4)[51] and to merge reads with FLASH (version 1.2.11)[52]. Then, MAGeCK (version 0.5.9.5)[53] was used to analyze the screening data. Specifically, the MAGeCK “count” command was employed to generate read counts for all samples, which were subsequently merged into a count matrix. The MAGeCK “test” command was then used to identify the top negatively and positively selected gRNAs or genes, using default settings. The software is available from https://sourceforge.net/projects/mageck/. Additionally, Gene Set Enrichment Analysis (GSEA) in the Kyoto Encyclopedia of Genes and Genomes (KEGG) functional pathway was performed using the GSEA() function from the R package clusterProfiler (version 3.12.0)[54], with default parameters. The KEGG database was selected from the “C2” category of the R package msigdbr (version 7.5.1), available at https://igordot.github.io/msigdbr/.

T7 endonuclease I (T7E1) assay

The T7E1 cleavage assay was performed using a previously reported protocol[55]. In brief, genomic DNA of infected OT-I T-cells were extracted and then subjected for PCR amplification of sgRNA targeting regions using primers indicated in Supplementary Table 3. PCR products were gel-purified using StarPrep DNA Gel Extraction kit (GenStar, Cat#D205-04), and annealed in 1xPCR buffer (TaKaRa,

Cat#9151A). The annealed products were incubated with 5 units of T7E1 (NEB, Cat#M0302L) at 37℃ for 20 minutes and then analyzed by PAGE.

Flow cytometry

For surface staining, cells were stained in 2% FBS/PBS on ice for 30 minutes. Intracellular staining was performed with a fixation/permeabilization kit (BD Biosciences) according to manufacturer's instructions. The following antibodies were used: APC anti-mouse CD8a (Invitrogen, 17-0081-83), PE anti-mouse CD279 (PD-1) (BioLegend, 109104), APC anti-mouse CD279 (PD-1) (BioLegend, 109112), PE-streptavidin (BioLegend, 405203), biotinylated erythrina cristagalli lectin (ECL) (B-1145-5), biotinylated succinylated wheat germ agglutinin (sWGA) (B-1025S-5), biotinylated recombinant Gal-1, APC anti-human CD8a (BioLegend, 300912). Flow cytometry was performed by BD FACSAria and data were analyzed with FlowJo.

ELISA

OT-I T-cells ($3x10^5$/ml) were co-cultured with B16F10-OVA cells at 37 °C for 8 hours in the presence of IL2 (2 ng/ml), IL7 (2.5 ng/ml), and IL15 (10 ng/ml). Supernatants were collected after co-culture. TNFα and IFNγ in the culture supernatant were measured using ELISA kits (ABclonal, Cat#RK00027, Cat#RK00019). Samples were plated in duplicate.

Human $CD8^+$ T-cells (3×10^5/ml) were co-cultured with A375 cells at 37 °C for 24 hours in the presence of human IL2 (500 IU/ml). Supernatants were collected for measurement of TNFα and IFNγ secretion using ELISA kits (ABclonal, Cat#RK00030, Cat#RK00015).

Mouse tumor models and adoptive transfer experiments

$4x10^5$ B16F10-OVA cells were injected subcutaneously into female C57BL/6J mice. Seven days post-injection, mice bearing tumors of similar size were randomly separated into 2 groups. A total of $2x10^6$ *B4galt1* gRNA-transduced or control

gRNA-transduced OT-I T-cells were injected intravenously. Tumors were then measured every two days with an electronic digital caliper. Tumor volume was calculated as width x width x length x 1/2.

Tumor-infiltrated lymphocyte (TIL) isolation

B16F10-OVA tumors were cut into small pieces in 6-well plates containing 5 ml RPMI 1640, 2% FBS, and 50 U/ml collagenase type IV (Invitrogen, V900893). Samples were incubated at 37 ℃ for 1 hour with rotation. Suspensions were passed through a 70 μm strainer and washed three times with PBS. Samples were then used for antibody staining and FACS analysis.

T-cell infiltration and proliferation within tumors

Following 4-day puromycin selection, infected OT-I T-cells were labeled with CFSE (carboxyfluorescein diacetate succinimidyl ester, Invitrogen), and $2x10^6$ labeled cells were intravenously transferred into Day 14 B16F10-OVA tumor-bearing mice. CFSE dilution was quantified by flow cytometry at 24 hours and Day 6 following transfer.

In vitro targeted cell killing

For OT-I T-cell killing activity assay, B16F10-OVA cells and B16F10 cells were labeled as $CFSE^{hi}$ (2.5 μM) and $CFSE^{lo}$ (50 nM), respectively, and then co-cultured with OT-I T-cells in 96-well plates at the indicated ratios. Cancer cells without addition of OT-I T-cells were used as controls. Following 24 hours of incubation, the ratios of $CFSE^{hi}$ and $CFSE^{lo}$ populations were detected by FACS.

Specific killing was calculated by following equation: specific killing percentage = [1-($CFSE^{hi}$/$CFSE^{lo}$ of T-cell)/($CFSE^{hi}$/$CFSE^{lo}$ of cancer cell only)] × 100%.

For NY-ESO-1 TCR-T and hCD19-CAR-T-cell in vitro killing assays, A375 cells and Nalm6 cells were co-cultured with T-cells for 24h and 8h, respectively. The killing percentage was calculated by following equation: killing percentage = [1-(survived target cell number / survived target cell number in non-T-cell wells)] × 100%.

Proteomic analysis of Gal-1 binding proteins in CD8$^+$ T-cells

Recombinant Gal-1 was purified[56] and coupled with Sepharose beads (Cat#GE17-0906-01). *B4galt1* knockout OT-I T-cells were co-cultured with MC38 for 8 hours and then stained by anti-Gal-1 antibody for sorting of Gal-1 negative OT-I T-cell population. Membrane extracts of OT-I T-cells were prepared by Mem-PER™ Plus Kit (Cat#89842Y). Extracts were incubated with Gal-1-Sepharose beads. After washing, binding proteins were eluted by 20 mM lactose and precipitated by DOC/TCA, and then separated on SDS-PAGE followed by silver staining (Sigma, PROTSIL1). The samples were digested and subjected to LC-MS (LTQ ORBITRAP Velos mass spectrometer, Thermo Fisher Scientific, San Jose, CA, USA).

Raw data was processed by Proteome Discoverer (version1.4, https://www.thermofisher.com/hk/en/home/industrial/mass-spectrometry/liquid-chromatography-mass-spectrometry-lc-ms/lc-ms-software/multi-omics-data-analysis/proteome-discoverer-software.html) to obtain a PSM (peptide spectrum matches) raw intensity table of all identified proteins for further analysis with R package DEqMS[57]. Raw intensity values were log2 transformed, and for each PSM, the median of log2 intensity was subtracted to get a relative log2 ratio. Then different expression of protein calculation was enabled in eBayes() function with method ROC (receiver operating characteristic) analysis. Differentially expressed proteins were selected by criteria $P < 0.05$. Those proteins were used for functional enrichment analysis with R package ClusterProfiler (version 3.12.0)[58] .

Western blot

10 μg cell membrane extracts of OT-I T-cells were separated by SDS-PAGE gels. Gels were transferred to nitrocellulose membranes (Amersham™ Protran®, Cat#10600001). Anti-CD8b (Abcam, Cat# ab228965) (1:1000), Anti-Ly9 (Abcam, Cat# ab252931) (1:1000), anti-Igf2g (Sino Biological, Cat# 107533-T40) (1:500), anti-Itgal (Solarbio, Cat# K002895P) (1:500), anti-Itgb7 (Solarbio, Cat#K004272P)

(1:500), anti-Lnpep (Santa Cruz, Cat#sc-365300) (1:100), and anti-Sell (Santa Cruz, Cat#sc-390756) (1:100) were used as primary antibodies. Secondary antibodies were IRDye® 680RD Donkey anti-Mouse IgG (LI-COR, P/N 926-68072) (1:10000), IRDye® 800CW Goat anti-Mouse IgG (LI-COR, P/N 926–32210) (1:10000), IRDye® 680RD Goat anti-Rabbit IgG (LI-COR, P/N 926-68071) (1:10000), IRDye® 800CW Goat anti-Rabbit IgG (LI-COR, P/N 926-32211) (1:10000). The membranes were scanned on an Odyssey imager (LI-COR).

FRET

TCR-CD8 FRET was measured by flow cytometry[30]. T-cells were incubated with PE-anti-Vα2 and APC-anti-CD8α at 4℃ for 30 minutes. Samples were stained with either antibody, both or neither. After staining, samples were fixed with fixation buffer at 4℃ for 10 minutes. FRET emission was assessed and FRET efficiency was calculated in FRET units as reported previously[30].

RT-qPCR and RNA-Seq

Total RNA was extracted using TRIzol® Reagent (Ambion, Cat# 15596018). cDNA was synthesized by the ImProm-II™ Reverse Transcriptase system (Promega, Cat# A3801) using 100 ng RNA per reaction. The qPCR reactions were prepared with TB Green® Premix Ex Taq™ (Takara, Cat# RR420A) using 1 µl cDNA per reaction in a 20 µl reaction volume. The relative gene expression levels were normalized to GAPDH.

Total RNA was used as input material for the RNA sample preparations. Sequencing libraries were generated using NEBNext Ultra RNA Library Prep Kit for Illumina (NEB, Catalog #E7530L) following manufacturer's recommendations and index codes were added to attribute sequences to each sample. Prepared libraries were quantified and sequenced by the Illumina NovaSeq 6000 S4 platform with 150 bp paired-end reads.

RNA-Seq data analysis

Raw data was aligned to mouse reference genome (mm10) with Ensemble version 98 gene annotation using TopHat2 (version 2.1.1). The raw count of each gene was then calculated using HTSeq (version 1.99.2)[59] and normalized to Fragments Per Kilobase of transcript per Million mapped reads (FPKM) by cufflinks (version 2.2.1)[60]. Differential gene expression analysis was performed using the R-based toolkit DESeq2 (version 1.38.0)[61], with differentially expressed genes (DEGs) defined by a significance threshold of P□<□0.05 or P□<□0.01. Functional enrichment analysis of these DEGs was conducted using the R package ClusterProfiler (version 3.12.0)[58].

Statistical analysis

Statistical analyses were conducted using R 4.1.0. Unless otherwise stated, statistical significance was determined using a two-tailed paired Student's t-test (*P < 0.05, **P < 0.01, ***P < 0.001; NS, not significant) with the function t.test(). Two-way ANOVA was performed using the function aov(). In the figures, the mean and standard error of the mean (SEM) are presented, with error bars representing the SEM value, calculated using the function sem().

Supplemental information

Supplemental information includes 9 figures and 5 tables.

Figure S1. Multiple components in N-glycan biosynthesis pathway were identified in genome-wide screenings for PD-1 regulators in CD8$^+$ T-cells.

a. Flow cytometry gating strategy for FACS sorting of ex vivo genome-wide screenings.
b. Schematic views of the N-glycan biosynthesis pathway. The genes identified in current genome-wide screenings are labeled.
c. Distribution of N-glycan biosynthesis-related genes in current screenings. The blue curve represents all target genes; the red curve represents all genes involved in the N-glycan biosynthesis pathway; and the gray curve represents control gRNAs.

d. Representative PD-1 FACS plots for gRNAs targeting B4galt1 (sg1 and sg2), Mgat2 (sg1 and sg2), and Dpm3 (sg1 and sg2) genes.

Figure S2. Gene knockout efficiency detected by T7E1 assay.

T7E1 assay showed gene knockout efficiencies of single sgRNAs validated in Fig. 1c and sgRNAs targeting B4galt1. * indicates the cleaved products.

Figure S3. Effect of B4GALT1 knockout on functions of hCD19-CAR-T-cells and anti-CD3/28 stimulated T-cells.

CRISPR/Cas9 knockout of B4GALT1 in hCD19-CAR-T-cells does not affect in vitro killing of Nalm6 target cells.

Data are shown as the mean ± SEM. NS, not significant.

Figure S4. Effect of B4GALT1 knockout on functions of anti-CD3/28 stimulated T-cells.

B4GALT1 knockout and control OT-I T-cells ($1X10^5$ cells/ml) were stimulated with anti-CD3 (1 mg/ml) and anti-CD28 (0.5 mg/ml) for 8 hours. The mRNA expression levels of Tnfα and Ifnγ were measured by quantitative RT-qPCR. The p-value was calculated using a two-tailed Student's t-test.

Data are shown as the mean ± SEM. **$P < 0.01$. NS, not significant.

Figure S5. Flow cytometry gating strategy for analysis of tumor-infiltrated OT-I T-cells.

Figure S6. Effect of B4GALT1 knockout on functions of tumor-infiltrated OT-I T-cells.

a. Tumor infiltration of CFSE-labeled OT-I $CD8^+$ T-cells 24 hours after transplantation. The p-value was calculated using a two-tailed Student's t-test.
b. Enhanced proliferation of CFSE-labeled B4GALT1 knockout (sgB4galt1) OT-I T-cells in tumors.

Data are shown as the mean ± SEM. NS, not significant.

Figure S7. CRISPR/Cas9 knockout of B4GALT1 in OT-I T-cells alters surface-binding of lectins and galectin-1.

a. Scheme for FACS analysis of N-glycome by lectins and galectin-1.

b-d. Cells were stained with biotin-ECL (b), biotin-sWGA (c), biotin-rGal-1 (d) and streptavidin-PE. Blue and red curves indicate control sgRNA- and sgB4galt1-infected OT-I cells, respectively. Gray dotted curves indicate cells stained with streptavidin-PE only. The MFIs of each sample were measured by FACS. The p-value was calculated using a two-tailed Student's t-test.

Data are shown as the mean ± SEM. *P < 0.05; **P < 0.01.

Figure S8. Flow cytometry gating strategy for TCR-CD8 FRET assay.

Figure S9. Expression levels of B4GALT1 and tumor-infiltrated $CD8^+$ T-cells in tumor microenvironment are associated with prognosis of human patients.

a. Kaplan-Meier survival curves of B4GALT1 expression levels for all primary tumor samples in TCGA cohort.
b. Kaplan-Meier survival curves of CD8A normalized B4GALT1 expression levels for all primary tumor samples in TCGA cohort.
c. The p-value heatmap showing associations between B4GALT1 expression levels and overall survival of patients with different tumor CD8A levels ($CD8A^{high}$ and $CD8A^{low}$) in indicated TCGA cohorts (three columns on the left), as well as associations between CD8A expression levels and overall survival of patients with different tumor B4GALT1 levels ($B4GALT1^{high}$ and $B4GATL1^{low}$) in indicated TCGA cohorts (three columns on the right). Hazard ratio (HR) values are listed in boxes. Samples with p-value > 0.05 were all filled with white background.

The p-values for all survival curves were calculated using two-sided Log-rank test.

Supplementary Table 1. List of sequences of gRNAs and primers used in current study.

Supplementary Table 2. List of plasmids used in current study.

Supplementary Table 3. Information of custom library used in current study.

Supplementary Table 4. Results of ex vivo CRISPR/Cas9 genome-wide screenings in Fig1b.

Supplementary Table 5. Results of in vivo CRISPR/Cas9 screenings with custom library in Fig2c.

References

1. Spencer KR, Wang J, Silk AW, Ganesan S, Kaufman HL,Mehnert JM. *Biomarkers for Immunotherapy: Current Developments and Challenges[J].* Am Soc Clin Oncol Educ Book, 2016. 35: p. e493-503.
2. Havel JJ, Chowell D,Chan TA. *The evolving landscape of biomarkers for checkpoint inhibitor immunotherapy[J].* Nat Rev Cancer, 2019. 19(3): p. 133-150.
3. Hodi FS, Mihm MC, Soiffer RJ, Haluska FG, Butler M, Seiden MV, Davis T, Henry-Spires R, MacRae S, Willman A, Padera R, Jaklitsch MT, Shankar S, Chen TC, Korman A, Allison JP,Dranoff G. *Biologic activity of cytotoxic T lymphocyte-associated antigen 4 antibody blockade in previously vaccinated metastatic melanoma and ovarian carcinoma patients[J].* Proc Natl Acad Sci U S A, 2003. 100(8): p. 4712-4717.
4. Brahmer JR, Tykodi SS, Chow LQ, Hwu WJ, Topalian SL, Hwu P, Drake CG, Camacho LH, Kauh J, Odunsi K, Pitot HC, Hamid O, Bhatia S, Martins R, Eaton K, Chen S, Salay TM, Alaparthy S, Grosso JF, Korman AJ, Parker SM, Agrawal S, Goldberg SM, Pardoll DM, Gupta A,Wigginton JM. *Safety and activity of anti-PD-L1 antibody in patients with advanced cancer[J].* N Engl J Med, 2012. 366(26): p. 2455-2465.
5. Topalian SL, Hodi FS, Brahmer JR, Gettinger SN, Smith DC, McDermott DF, Powderly JD, Carvajal RD, Sosman JA, Atkins MB, Leming PD, Spigel DR, Antonia SJ, Horn L, Drake CG, Pardoll DM, Chen L, Sharfman WH, Anders RA, Taube JM, McMiller TL, Xu H, Korman AJ, Jure-Kunkel M, Agrawal S, McDonald D, Kollia GD, Gupta A, Wigginton JM,Sznol M. *Safety, activity, and immune correlates of anti-PD-1 antibody in cancer[J].* N Engl J Med, 2012. 366(26): p. 2443-2454.
6. Ribas A,Wolchok JD. *Cancer immunotherapy using checkpoint blockade[J].* Science, 2018. 359(6382): p. 1350-1355.
7. Cercek A, Lumish M, Sinopoli J, Weiss J, Shia J, Lamendola-Essel M, El Dika IH, Segal N, Shcherba M, Sugarman R, Stadler Z, Yaeger R, Smith JJ, Rousseau B, Argiles G, Patel M, Desai A, Saltz LB, Widmar M, Iyer K, Zhang J, Gianino N, Crane C, Romesser PB, Pappou EP, Paty P, Garcia-Aguilar J, Gonen M, Gollub M, Weiser MR, Schalper KA,Diaz LA, Jr. *PD-1 Blockade in Mismatch Repair-Deficient, Locally Advanced Rectal Cancer[J].* N Engl J Med, 2022.
8. June CH, O'Connor RS, Kawalekar OU, Ghassemi S,Milone MC. *CAR T cell immunotherapy for human cancer[J].* Science, 2018. 359(6382): p. 1361-1365.
9. Rafiq S, Hackett CS,Brentjens RJ. *Engineering strategies to overcome the current roadblocks in CAR T cell therapy[J].* Nat Rev Clin Oncol, 2020. 17(3): p. 147-167.
10. Agata Y, Kawasaki A, Nishimura H, Ishida Y, Tsubata T, Yagita H,Honjo T. *Expression of the PD-1 antigen on the surface of stimulated mouse T and B lymphocytes[J].* Int Immunol, 1996. 8(5): p. 765-772.
11. Yu Y, Tsang JC, Wang C, Clare S, Wang J, Chen X, Brandt C, Kane L, Campos LS, Lu L, Belz GT, McKenzie AN, Teichmann SA, Dougan G,Liu P. *Single-cell RNA-seq identifies a PD-1(hi) ILC progenitor and defines its development pathway[J].*

Nature, 2016. 539(7627): p. 102-106.
12. Gordon SR, Maute RL, Dulken BW, Hutter G, George BM, McCracken MN, Gupta R, Tsai JM, Sinha R, Corey D, Ring AM, Connolly AJ,Weissman IL. *PD-1 expression by tumour-associated macrophages inhibits phagocytosis and tumour immunity[J].* Nature, 2017. 545(7655): p. 495-499.
13. Park BV, Freeman ZT, Ghasemzadeh A, Chattergoon MA, Rutebemberwa A, Steigner J, Winter ME, Huynh TV, Sebald SM, Lee SJ, Pan F, Pardoll DM,Cox AL. *TGFbeta1-Mediated SMAD3 Enhances PD-1 Expression on Antigen-Specific T Cells in Cancer[J].* Cancer Discov, 2016. 6(12): p. 1366-1381.
14. Stephen TL, Payne KK, Chaurio RA, Allegrezza MJ, Zhu H, Perez-Sanz J, Perales-Puchalt A, Nguyen JM, Vara-Ailor AE, Eruslanov EB, Borowsky ME, Zhang R, Laufer TM,Conejo-Garcia JR. *SATB1 Expression Governs Epigenetic Repression of PD-1 in Tumor-Reactive T Cells[J].* Immunity, 2017. 46(1): p. 51-64.
15. Okada M, Chikuma S, Kondo T, Hibino S, Machiyama H, Yokosuka T, Nakano M,Yoshimura A. *Blockage of Core Fucosylation Reduces Cell-Surface Expression of PD-1 and Promotes Anti-tumor Immune Responses of T Cells[J].* Cell Rep, 2017. 20(5): p. 1017-1028.
16. Meng X, Liu X, Guo X, Jiang S, Chen T, Hu Z, Liu H, Bai Y, Xue M, Hu R, Sun SC, Zhou P, Huang X, Wei L, Yang W,Xu C. *FBXO38 mediates PD-1 ubiquitination and regulates anti-tumour immunity of T cells[J].* Nature, 2018. 564(7734): p. 130-135.
17. Zhou XA, Zhou J, Zhao L, Yu G, Zhan J, Shi C, Yuan R, Wang Y, Chen C, Zhang W, Xu D, Ye Y, Wang W, Shen Z,Wang J. *KLHL22 maintains PD-1 homeostasis and prevents excessive T cell suppression[J].* Proc Natl Acad Sci U S A, 2020. 117(45): p. 28239-28250.
18. Wei J, Long L, Zheng W, Dhungana Y, Lim SA, Guy C, Wang Y, Wang YD, Qian C, Xu B, Kc A, Saravia J, Huang H, Yu J, Doench JG, Geiger TL,Chi H. *Targeting REGNASE-1 programs long-lived effector T cells for cancer therapy[J].* Nature, 2019. 576(7787): p. 471-476.
19. Zhao H, Liu Y, Wang L, Jin G, Zhao X, Xu J, Zhang G, Ma Y, Yin N,Peng M. *Genome-wide fitness gene identification reveals Roquin as a potent suppressor of CD8 T cell expansion and anti-tumor immunity[J].* Cell Rep, 2021. 37(10): p. 110083.
20. Ma X, Xiao L, Liu L, Ye L, Su P, Bi E, Wang Q, Yang M, Qian J,Yi Q. *CD36-mediated ferroptosis dampens intratumoral CD8(+) T cell effector function and impairs their antitumor ability[J].* Cell Metab, 2021. 33(5): p. 1001-1012 e1005.
21. Xu S, Chaudhary O, Rodriguez-Morales P, Sun X, Chen D, Zappasodi R, Xu Z, Pinto AFM, Williams A, Schulze I, Farsakoglu Y, Varanasi SK, Low JS, Tang W, Wang H, McDonald B, Tripple V, Downes M, Evans RM, Abumrad NA, Merghoub T, Wolchok JD, Shokhirev MN, Ho PC, Witztum JL, Emu B, Cui G,Kaech SM. *Uptake of oxidized lipids by the scavenger receptor CD36 promotes lipid peroxidation and dysfunction in CD8(+) T cells in tumors[J].* Immunity, 2021. 54(7): p. 1561-1577 e1567.
22. Rodeheffer C,Shur BD. *Targeted mutations in beta1,4-galactosyltransferase I*

reveal its multiple cellular functions[J]. Biochim Biophys Acta, 2002. 1573(3): p. 258-270.

23. Cheng X, Wang X, Han Y,Wu Y. *The expression and function of beta-1,4-galactosyltransferase-I in dendritic cells[J].* Cell Immunol, 2010. 266(1): p. 32-39.

24. Han Y, Zhou X, Ji Y, Shen A, Sun X, Hu Y, Wu Q,Wang X. *Expression of beta-1,4-galactosyltransferase-I affects cellular adhesion in human peripheral blood CD4+ T cells[J].* Cell Immunol, 2010. 262(1): p. 11-17.

25. Gomez-Henao W, Tenorio EP, Sanchez FRC, Mendoza MC, Ledezma RL,Zenteno E. *Relevance of glycans in the interaction between T lymphocyte and the antigen presenting cell[J].* Int Rev Immunol, 2021. 40(4): p. 274-288.

26. Cui Y, Li J, Zhang P, Yin D, Wang Z, Dai J, Wang W, Zhang E,Guo R. *B4GALT1 promotes immune escape by regulating the expression of PD-L1 at multiple levels in lung adenocarcinoma[J].* J Exp Clin Cancer Res, 2023. 42(1): p. 146.

27. Hsu TH, Chang YC, Lee YY, Chen CL, Hsiao M, Lin FR, Chen LH, Lin CH, Angata T, Liu FT,Lin KI. *B4GALT1-dependent galectin-8 binding with TGF-beta receptor suppresses colorectal cancer progression and metastasis[J].* Cell Death Dis, 2024. 15(9): p. 654.

28. De Vitis C, Corleone G, Salvati V, Ascenzi F, Pallocca M, De Nicola F, Fanciulli M, di Martino S, Bruschini S, Napoli C, Ricci A, Bassi M, Venuta F, Rendina EA, Ciliberto G,Mancini R. *B4GALT1 Is a New Candidate to Maintain the Stemness of Lung Cancer Stem Cells[J].* J Clin Med, 2019. 8(11).

29. Robbins PF, Li YF, El-Gamil M, Zhao Y, Wargo JA, Zheng Z, Xu H, Morgan RA, Feldman SA, Johnson LA, Bennett AD, Dunn SM, Mahon TM, Jakobsen BK,Rosenberg SA. *Single and dual amino acid substitutions in TCR CDRs can enhance antigen-specific T cell functions[J].* J Immunol, 2008. 180(9): p. 6116-6131.

30. Smith LK, Boukhaled GM, Condotta SA, Mazouz S, Guthmiller JJ, Vijay R, Butler NS, Bruneau J, Shoukry NH, Krawczyk CM,Richer MJ. *Interleukin-10 Directly Inhibits CD8(+) T Cell Function by Enhancing N-Glycan Branching to Decrease Antigen Sensitivity[J].* Immunity, 2018. 48(2): p. 299-312 e295.

31. Borger JG, Zamoyska R,Gakamsky DM. *Proximity of TCR and its CD8 coreceptor controls sensitivity of T cells[J].* Immunol Lett, 2014. 157(1-2): p. 16-22.

32. Weinstein JN, Collisson EA, Mills GB, Shaw KR, Ozenberger BA, Ellrott K, Shmulevich I, Sander C,Stuart JM. *The Cancer Genome Atlas Pan-Cancer analysis project[J].* Nat Genet, 2013. 45(10): p. 1113-1120.

33. Tang Z, Kang B, Li C, Chen T,Zhang Z. *GEPIA2: an enhanced web server for large-scale expression profiling and interactive analysis[J].* Nucleic Acids Res, 2019. 47(W1): p. W556-W560.

34. Pan YM,Cheng YX. *Splicing factor proline- and glutamine-rich regulates cytotoxic T lymphocytes-mediated cytotoxicity on non-small cell lung cancer by directly binding to PD-L1 3'UTR[J].* Medicine, 2023. 102(45).

35. Coulie PG, Van den Eynde BJ, van der Bruggen P,Boon T. *Tumour antigens*

recognized by T lymphocytes: at the core of cancer immunotherapy[J]. Nature Reviews Cancer, 2014. 14(2): p. 135-146.

36. Keir ME, Butte MJ, Freeman GJ,Sharpe AH. *PD-1 and its ligands in tolerance and immunity[J].* Annu Rev Immunol, 2008. 26: p. 677-704.

37. Frontiers Production O. *Erratum: CD8 T cell function and cross-reactivity explored by stepwise increased peptide-HLA versus TCR affinity[J].* Front Immunol, 2023. 14: p. 1178295.

38. Kinter AL, Godbout EJ, McNally JP, Sereti I, Roby GA, O'Shea MA,Fauci AS. *The common gamma-chain cytokines IL-2, IL-7, IL-15, and IL-21 induce the expression of programmed death-1 and its ligands[J].* J Immunol, 2008. 181(10): p. 6738-6746.

39. Dong H, Zhu G, Tamada K,Chen L. *B7-H1, a third member of the B7 family, co-stimulates T-cell proliferation and interleukin-10 secretion[J].* Nat Med, 1999. 5(12): p. 1365-1369.

40. Jiang Y, Li Y,Zhu B. *T-cell exhaustion in the tumor microenvironment[J].* Cell Death Dis, 2015. 6(6): p. e1792.

41. Kamphorst AO, Wieland A, Nasti T, Yang S, Zhang R, Barber DL, Konieczny BT, Daugherty CZ, Koenig L, Yu K, Sica GL, Sharpe AH, Freeman GJ, Blazar BR, Turka LA, Owonikoko TK, Pillai RN, Ramalingam SS, Araki K,Ahmed R. *Rescue of exhausted CD8 T cells by PD-1-targeted therapies is CD28-dependent[J].* Science, 2017. 355(6332): p. 1423-1427.

42. Sharpe AH,Pauken KE. *The diverse functions of the PD1 inhibitory pathway[J].* Nat Rev Immunol, 2018. 18(3): p. 153-167.

43. Abdelbary M,Nolz JC. *N-linked glycans: an underappreciated key determinant of T cell development, activation, and function[J].* Immunometabolism (Cobham), 2023. 5(4): p. e00035.

44. Kalos M,June CH. *Adoptive T cell transfer for cancer immunotherapy in the era of synthetic biology[J].* Immunity, 2013. 39(1): p. 49-60.

45. Kamphorst AO,Ahmed R. *CD4 T-cell immunotherapy for chronic viral infections and cancer[J].* Immunotherapy, 2013. 5(9): p. 975-987.

46. Sterner RC,Sterner RM. *CAR-T cell therapy: current limitations and potential strategies[J].* Blood Cancer J, 2021. 11(4): p. 69.

47. Zhang T, Tai Z, Miao F, Zhang X, Li J, Zhu Q, Wei H,Chen Z. *Adoptive cell therapy for solid tumors beyond CAR-T: Current challenges and emerging therapeutic advances[J].* J Control Release, 2024. 368: p. 372-396.

48. Wu R, Forget MA, Chacon J, Bernatchez C, Haymaker C, Chen JQ, Hwu P,Radvanyi LG. *Adoptive T-cell therapy using autologous tumor-infiltrating lymphocytes for metastatic melanoma: current status and future outlook[J].* Cancer J, 2012. 18(2): p. 160-175.

49. Platt RJ, Chen S, Zhou Y, Yim MJ, Swiech L, Kempton HR, Dahlman JE, Parnas O, Eisenhaure TM, Jovanovic M, Graham DB, Jhunjhunwala S, Heidenreich M, Xavier RJ, Langer R, Anderson DG, Hacohen N, Regev A, Feng G, Sharp PA,Zhang F. *CRISPR-Cas9 knockin mice for genome editing and cancer modeling[J].* Cell, 2014.

159(2): p. 440-455.

50. Kurachi M, Kurachi J, Chen Z, Johnson J, Khan O, Bengsch B, Stelekati E, Attanasio J, McLane LM, Tomura M, Ueha S,Wherry EJ. *Optimized retroviral transduction of mouse T cells for in vivo assessment of gene function[J].* Nat Protoc, 2017. 12(9): p. 1980-1998.

51. Martin M. *Cutadapt removes adapter sequences from high-throughput sequencing reads[J].* EMBnet. journal, 2011. 17(1): p. 10-12.

52. Magoc T,Salzberg SL. *FLASH: fast length adjustment of short reads to improve genome assemblies[J].* Bioinformatics, 2011. 27(21): p. 2957-2963.

53. Li W, Xu H, Xiao T, Cong L, Love MI, Zhang F, Irizarry RA, Liu JS, Brown M,Liu XS. *MAGeCK enables robust identification of essential genes from genome-scale CRISPR/Cas9 knockout screens[J].* Genome Biol, 2014. 15(12): p. 554.

54. Yu G, Wang L-G, Han Y,He Q-Y. *clusterProfiler: an R package for comparing biological themes among gene clusters[J].* Omics: a journal of integrative biology, 2012. 16(5): p. 284-287.

55. Duan J, Lu G, Xie Z, Lou M, Luo J, Guo L,Zhang Y. *Genome-wide identification of CRISPR/Cas9 off-targets in human genome[J].* Cell Res, 2014. 24(8): p. 1009-1012.

56. Prato CA, Carabelli J, Cattaneo V, Campetella O,Tribulatti MV. *Purification of recombinant galectins expressed in bacteria[J].* STAR protocols, 2020. 1(3): p. 100204.

57. Zhu Y, Orre LM, Zhou Tran Y, Mermelekas G, Johansson HJ, Malyutina A, Anders S,Lehtio J. *DEqMS: A Method for Accurate Variance Estimation in Differential Protein Expression Analysis[J].* Mol Cell Proteomics, 2020. 19(6): p. 1047-1057.

58. Wu T, Hu E, Xu S, Chen M, Guo P, Dai Z, Feng T, Zhou L, Tang W, Zhan L, Fu X, Liu S, Bo X,Yu G. *clusterProfiler 4.0: A universal enrichment tool for interpreting omics data[J].* Innovation (Camb), 2021. 2(3): p. 100141.

59. Putri GH, Anders S, Pyl PT, Pimanda JE,Zanini F. *Analysing high-throughput sequencing data in Python with HTSeq 2.0[J].* Bioinformatics, 2022. 38(10): p. 2943-2945.

60. Trapnell C, Roberts A, Goff L, Pertea G, Kim D, Kelley DR, Pimentel H, Salzberg SL, Rinn JL,Pachter L. *Differential gene and transcript expression analysis of RNA-seq experiments with TopHat and Cufflinks[J].* Nat Protoc, 2012. 7(3): p. 562-578.

61. Love MI, Huber W,Anders S. *Moderated estimation of fold change and dispersion for RNA-seq data with DESeq2[J].* Genome Biol, 2014. 15(12): p. 550.

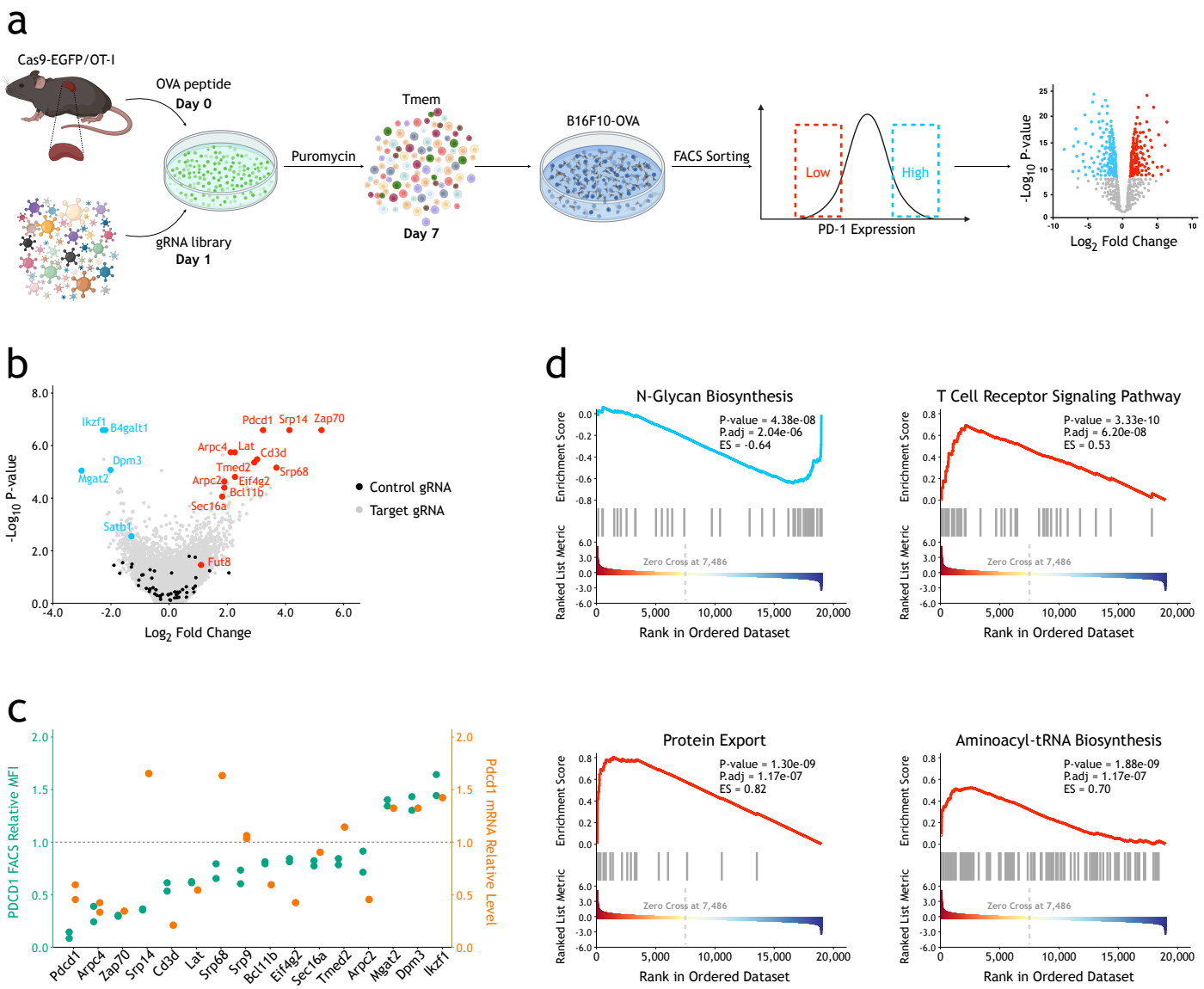
a
Cas9-EGFP/OT-I
OVA peptide
Day 0
gRNA library
Day 1
Puromycin
Tmem
Day 7
B16F10-OVA
FACS Sorting
Low
High
PD-1 Expression
-Log10 P-value
Log2 Fold Change
b
-Log10 P-value
Log2 Fold Change
Ikzf1
B4galt1
Dpm3
Mgat2
Satb1
Pdcd1
Srp14
Zap70
Arpc4
Lat
Cd3d
Tmed2
Srp68
Arpc2
Eif4g2
Bcl11b
Sec16a
Fut8
Control gRNA
Target gRNA
c
PDCD1 FACS Relative MFI
Pdcd1 mRNA Relative Level
Pdcd1
Arpc4
Zap70
Srp14
Cd3d
Lat
Srp68
Srp9
Bcl11b
Eif4g2
Sec16a
Tmed2
Arpc2
Mgat2
Dpm3
Ikzf1
d
N-Glycan Biosynthesis
P-value = 4.38e-08
P.adj = 2.04e-06
ES = -0.64
T Cell Receptor Signaling Pathway
P-value = 3.33e-10
P.adj = 6.20e-08
ES = 0.53
Protein Export
P-value = 1.30e-09
P.adj = 1.17e-07
ES = 0.82
Aminoacyl-tRNA Biosynthesis
P-value = 1.88e-09
P.adj = 1.17e-07
ES = 0.70
Enrichment Score
Ranked List Metric
Zero Cross at 7,486
Rank in Ordered Dataset

Figure 1

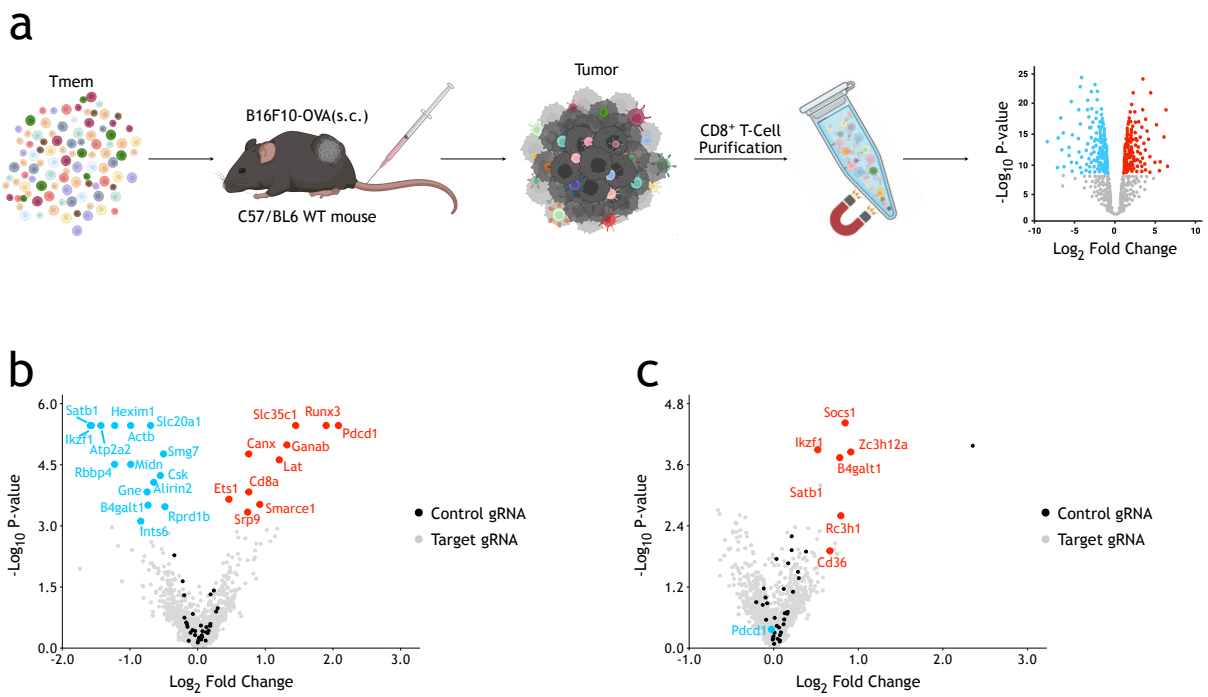
a
Tmem
B16F10-OVA(s.c.)
C57/BL6 WT mouse
Tumor
CD8+ T-Cell
Purification
-Log10 P-value
Log2 Fold Change
b
Satb1
Hexim1
Slc20a1
Ikzf1
Actb
Atp2a2
Smg7
Rbbp4
Midn
Csk
Gne
Alirin2
B4galt1
Rprd1b
Ints6
Slc35c1
Runx3
Pdcd1
Canx
Ganab
Lat
Cd8a
Ets1
Smarce1
Srp9
Control gRNA
Target gRNA
-Log10 P-value
Log2 Fold Change
c
Socs1
Ikzf1
Zc3h12a
B4galt1
Satb1
Rc3h1
Cd36
Pdcd1
Control gRNA
Target gRNA
-Log10 P-value
Log2 Fold Change

Figure 2

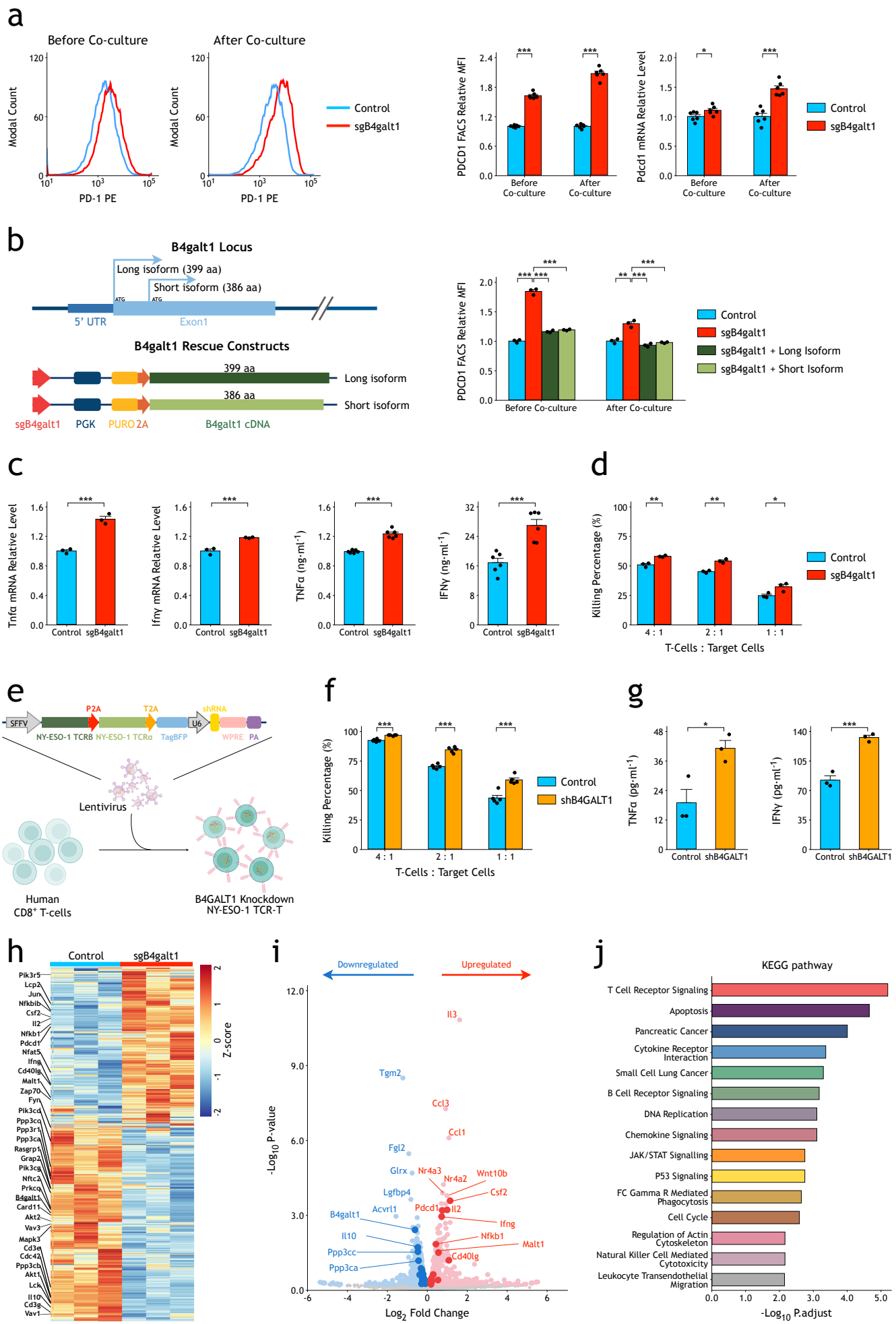
a
Before Co-culture
After Co-culture
Modal Count
PD-1 PE
Control
sgB4galt1
PDCD1 FACS Relative MFI
Pdcd1 mRNA Relative Level
Before Co-culture
After Co-culture
b
B4galt1 Locus
Long isoform (399 aa)
Short isoform (386 aa)
5' UTR
Exon1
B4galt1 Rescue Constructs
399 aa
386 aa
Long isoform
Short isoform
sgB4galt1
PGK
PURO 2A
B4galt1 cDNA
sgB4galt1 + Long Isoform
sgB4galt1 + Short Isoform
c
Tnfα mRNA Relative Level
Ifnγ mRNA Relative Level
TNFα (ng·ml⁻¹)
IFNγ (ng·ml⁻¹)
d
Killing Percentage (%)
T-Cells : Target Cells
e
SFFV
P2A
T2A
shRNA
U6
NY-ESO-1 TCRB
NY-ESO-1 TCRα
TagBFP
WPRE
PA
Lentivirus
Human CD8⁺ T-cells
B4GALT1 Knockdown NY-ESO-1 TCR-T
f
shB4GALT1
g
h
Z-score
i
Downregulated
Upregulated
-Log10 P-value
Log2 Fold Change
j
KEGG pathway
T Cell Receptor Signaling
Apoptosis
Pancreatic Cancer
Cytokine Receptor Interaction
Small Cell Lung Cancer
B Cell Receptor Signaling
DNA Replication
Chemokine Signaling
JAK/STAT Signalling
P53 Signaling
FC Gamma R Mediated Phagocytosis
Cell Cycle
Regulation of Actin Cytoskeleton
Natural Killer Cell Mediated Cytotoxicity
Leukocyte Transendothelial Migration
-Log10 P.adjust

Figure 3

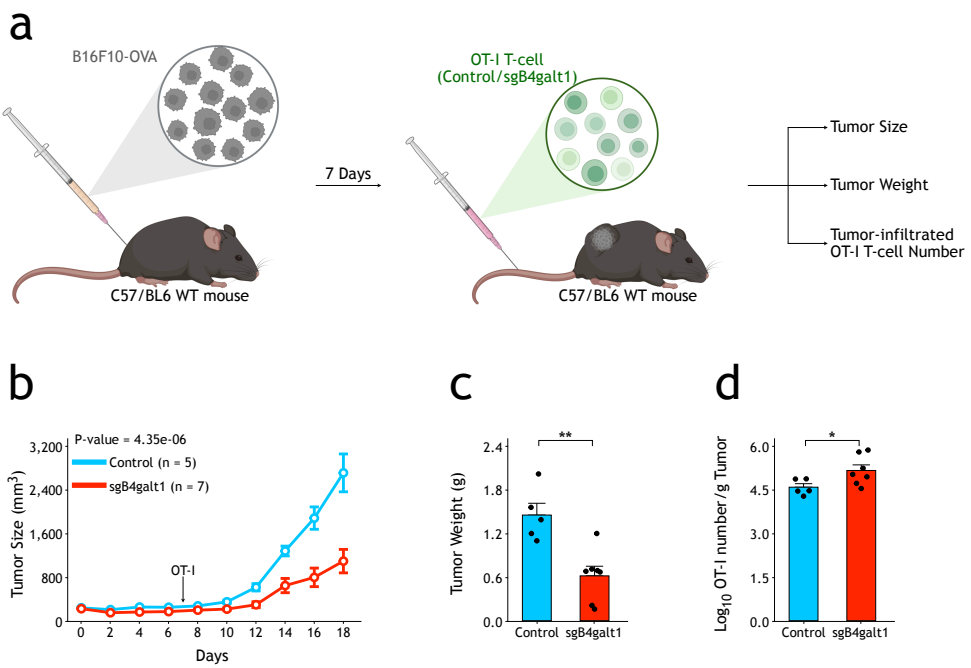
a
B16F10-OVA
C57/BL6 WT mouse
7 Days
OT-I T-cell
(Control/sgB4galt1)
C57/BL6 WT mouse
Tumor Size
Tumor Weight
Tumor-infiltrated
OT-I T-cell Number
b
P-value = 4.35e-06
Control (n = 5)
sgB4galt1 (n = 7)
Tumor Size (mm3)
OT-I
Days
c
Tumor Weight (g)
Control
sgB4galt1
d
Log10 OT-I number/g Tumor
Control
sgB4galt1

Figure 4

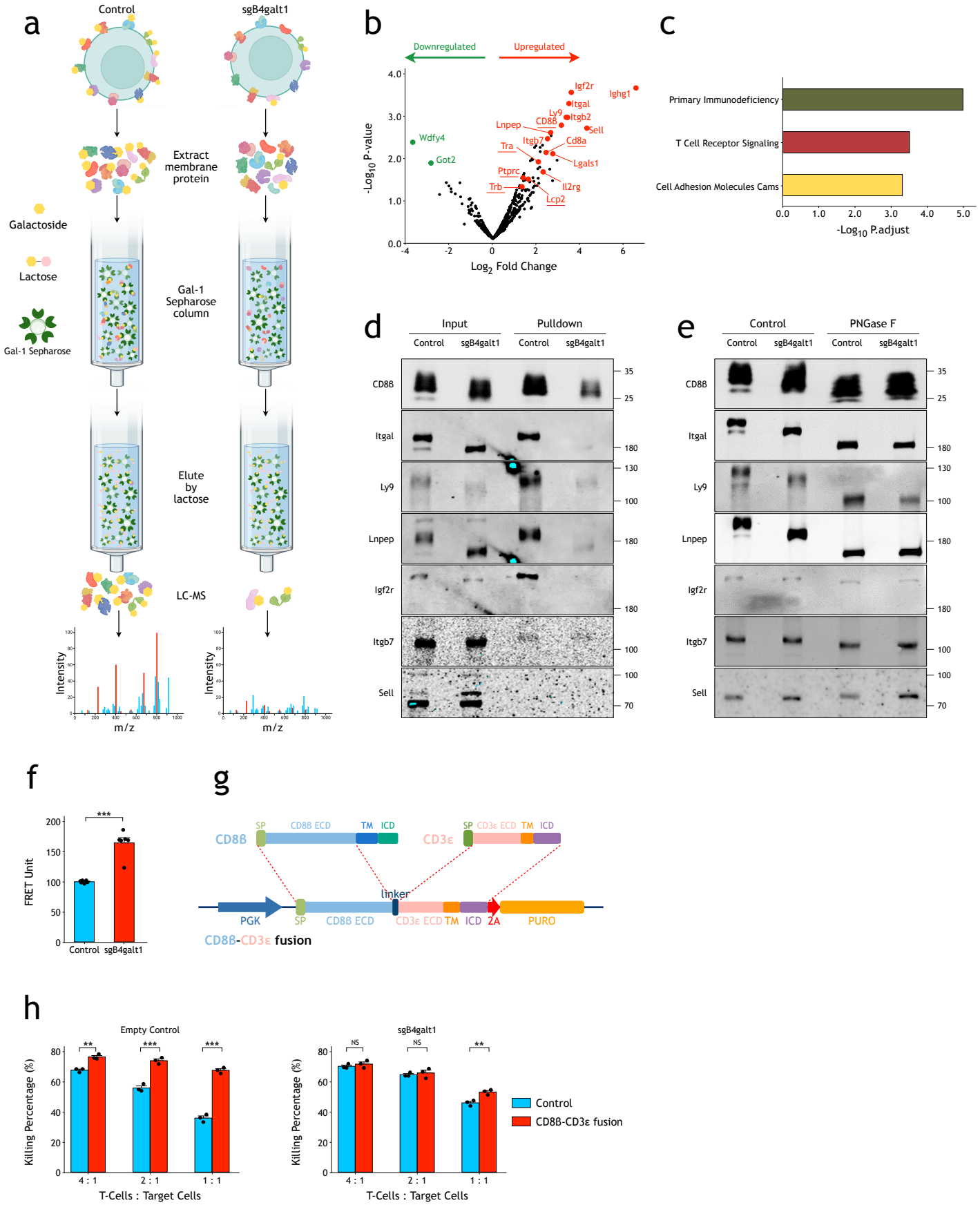
a
Control
sgB4galt1
Extract membrane protein
Galactoside
Lactose
Gal-1 Sepharose
Gal-1 Sepharose column
Elute by lactose
LC-MS
Intensity
m/z
b
Downregulated
Upregulated
-Log10 P-value
Log2 Fold Change
Igf2r
Ighg1
Itgal
Ly9
Itgb2
CD8B
Sell
Lnpep
Wdfy4
Itgb7
Cd8a
Tra
Got2
Lgals1
Ptprc
Il2rg
Trb
Lcp2
c
Primary Immunodeficiency
T Cell Receptor Signaling
Cell Adhesion Molecules Cams
-Log10 P.adjust
d
Input
Pulldown
Control
sgB4galt1
CD8B
Itgal
Ly9
Lnpep
Igf2r
Itgb7
Sell
e
Control
PNGase F
f
FRET Unit
Control
sgB4galt1
g
CD8B
SP
CD8B ECD
TM
ICD
CD3ε
CD3ε ECD
linker
PGK
2A
PURO
CD8B-CD3ε fusion
h
Empty Control
sgB4galt1
Killing Percentage (%)
T-Cells : Target Cells
4 : 1
2 : 1
1 : 1
NS
Control
CD8B-CD3ε fusion

Figure 5

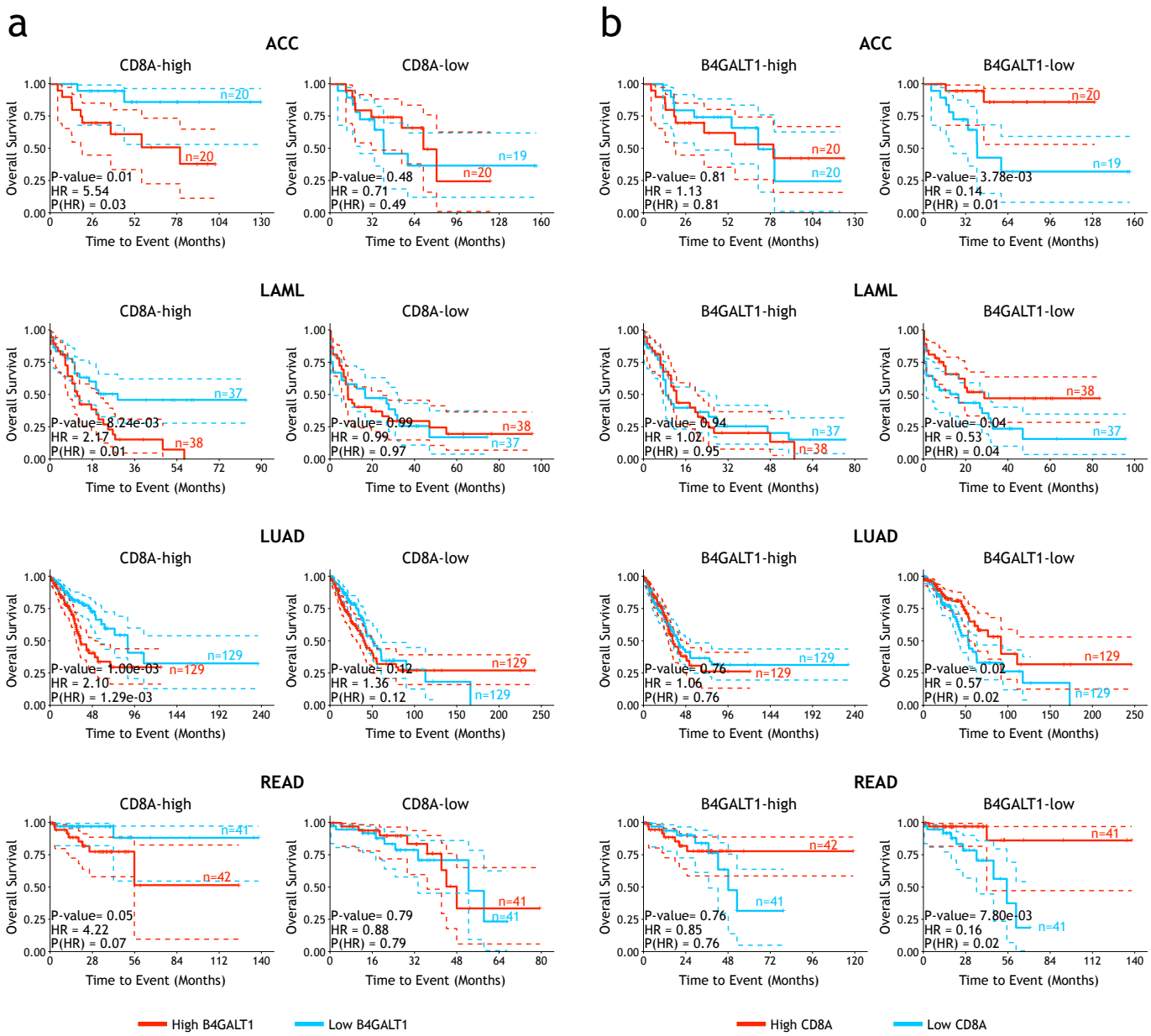
a
ACC
CD8A-high
P-value= 0.01
HR = 5.54
P(HR) = 0.03
n=20
n=20
CD8A-low
P-value= 0.48
HR = 0.71
P(HR) = 0.49
n=19
n=20
LAML
CD8A-high
P-value= 8.24e-03
HR = 2.17
P(HR) = 0.01
n=37
n=38
CD8A-low
P-value= 0.99
HR = 0.99
P(HR) = 0.97
n=38
n=37
LUAD
CD8A-high
P-value= 1.00e-03
HR = 2.10
P(HR) = 1.29e-03
n=129
n=129
CD8A-low
P-value= 0.12
HR = 1.36
P(HR) = 0.12
n=129
n=129
READ
CD8A-high
P-value= 0.05
HR = 4.22
P(HR) = 0.07
n=41
n=42
CD8A-low
P-value= 0.79
HR = 0.88
P(HR) = 0.79
n=41
n=41
High B4GALT1
Low B4GALT1
b
ACC
B4GALT1-high
P-value= 0.81
HR = 1.13
P(HR) = 0.81
n=20
n=20
B4GALT1-low
P-value= 3.78e-03
HR = 0.14
P(HR) = 0.01
n=20
n=19
LAML
B4GALT1-high
P-value= 0.94
HR = 1.02
P(HR) = 0.95
n=37
n=38
B4GALT1-low
P-value= 0.04
HR = 0.53
P(HR) = 0.04
n=38
n=37
LUAD
B4GALT1-high
P-value= 0.76
HR = 1.06
P(HR) = 0.76
n=129
n=129
B4GALT1-low
P-value= 0.02
HR = 0.57
P(HR) = 0.02
n=129
n=129
READ
B4GALT1-high
P-value= 0.76
HR = 0.85
P(HR) = 0.76
n=42
n=41
B4GALT1-low
P-value= 7.80e-03
HR = 0.16
P(HR) = 0.02
n=41
n=41
High CD8A
Low CD8A
Overall Survival
Time to Event (Months)

Figure 6